PTCHD1 interacts with the SNARE-associated protein SNAPIN *in vitro* via its first exoplasmic loop

Stephen F. Pastore[1,2], Connie T.Y. Xie[6], Tahir Muhammad[1,2], Sierra C. El-masri[1], Paul W. Frankland[2,3,4,5], Paul A. Hamel[6], John B. Vincent[1,2,7]

[1]Molecular Neuropsychiatry & Development (MiND) Lab, Molecular Brain Science Research Department, Campbell Family Mental Health Research Institute, Centre for Addiction and Mental Health, Toronto, ON, M5T 1RS, Canada;

[2]Institute of Medical Science, University of Toronto, Toronto, ON, M5S 1A8, Canada;

[3]Program in Neurosciences and Mental Health, The Hospital for Sick Children, Toronto, Ontario, Canada, M5G 1X8;

[4]Department of Physiology, University of Toronto, Toronto, Ontario, Canada, M5S 1A8;

[5]Department of Psychology, University of Toronto, Toronto, Ontario, Canada, M5S 3G3;

[6]Department of Laboratory Medicine & Pathobiology, University of Toronto, Toronto, ON, M5S 1A8, Canada;

[7]Department of Psychiatry, University of Toronto, Toronto, ON, M5T 1R8, Canada.

*Correspondence should be addressed to: Dr. John B. Vincent, Molecular Brain Science Research Department, Campbell Family Mental Health Research Institute, Centre for Addiction and Mental Health (CAMH), 250 College Street, Toronto, ON, Canada, M5T 1R8; Email: john.vincent@camh.ca

ABSTRACT

Patched domain-containing 1 (*PTCHD1*) is a susceptibility gene for autism spectrum disorder (ASD) and intellectual disability (ID). PTCHD1 is predicted to encode a multi-pass protein consisting of 12 transmembrane domains, two large exoplasmic loops, and a C-terminal PDZ-binding domain. PTCHD1 contains sequence homology with the Hedgehog signaling pathway repressors Patched domain-containing-1 (PTCH1) and -2 (PTCH2), as well as the cholesterol trafficking protein Niemann-Pick disease type C1 (NPC1). Despite this homology, the functional role of PTCHD1 in brain development remains elusive. Studies have sought to characterize the function of PTCHD1 by elucidating its neural network of interacting proteins. Using a yeast two-hybrid assay, we have identified a novel interaction between the first exoplasmic loop of PTCHD1 and the SNARE-associated protein SNAPIN, which is implicated in synaptic vesicle exocytosis. Clinically-associated missense variants within this region of *PTCHD1* did not disrupt SNAPIN binding, indicating that the pathoetiology of these variants is unrelated to this interaction. However, several of these missense variants exhibited pronounced retention within the endoplasmic reticulum, and impaired trafficking to the plasma membrane, indicating a possible mechanism of pathogenicity. These data yield insights regarding the possible role of PTCHD1 in neurodevelopment and neurotransmission, as well as suggest a pathoetiological mechanism for numerous clinical missense variants, providing a platform for subsequent diagnostic assays, and an avenue for possible therapeutic intervention.

1. Introduction

Autism spectrum Disorder (ASD) is a heterogeneous neurodevelopmental disorder typified by social and communicative deficiencies, restricted interests, and repetitive sensory-motor behaviours[1]. The worldwide incidence of ASD has been estimated to be roughly one percent[2], with males displaying an approximately three-fold higher prevalence than females[3]. ASD also exhibits 50-80% comorbidity with intellectual disability (ID)[4]. Genetics appear to strongly influence the pathoetiology of ASD, with a recent meta-analysis of twin studies concluding that 74-93% of ASD risk is heritable[5]. Consequently, many genome-wide studies of affected cohorts have identified various ASD and ID susceptibility genes. Patched domain-containing 1 (*PTCHD1*) (MIM: 300828) is encoded on the X-chromosome at the locus Xp22.11 in humans, and was first implicated in the pathoetiology of ASD and ID in 2008[6]. Numerous highly-penetrant rare genomic loss variants and loss-of-function (LoF) coding variants have been subsequently identified[7]. In addition, many missense variants have been identified through clinical diagnostics (for example see ClinVar: https://www.ncbi.nlm.nih.gov/clinvar), however the vast majority of these are interpreted as variants of uncertain significance due to the lack of supporting segregation data or functional data. This diagnostic uncertainty negatively impacts the healthcare options available to families.

In silico analyses have predicted PTCHD1 to be a multi-pass protein consisting of 12 transmembrane domains. Exogenously expressed PTCHD1 has correspondingly been found to localize within cell membranes[8–10], and is specifically targeted to the dendritic spines of neurons[9]. In addition, PTCHD1 is predicted to possess two distinct sterol-sensing domains, two large exoplasmic loops, and a C-terminal PDZ-binding domain[7]. Missense variants in ASD or ID individuals have been identified which involve evolutionarily-conserved amino acids located within the first transmembrane domain (Pro32Arg

and Pro32Leu), first lumenal loop (Lys181Thr and Tyr213Cys), and third transmembrane domain (Gly300Arg and Ala310Pro) have displayed retention by the endoplasmic reticulum (ER), diminished cell membrane trafficking, and attenuated protein expression[10]. Similarly, the missense variants Pro32Arg, Gly303Arg (third transmembrane domain), and Phe549Cys (second lumenal loop) do not appear to undergo correct post-translational processing in the ER, as evidenced by the absence of mature N-linked glycans present on these variants[11].

Functionally, a definitive cellular role of PTCHD1 has yet to be elucidated. PTCHD1 demonstrates 21.62% and 20.65% sequence homology with the Patched domain-containing proteins Patched-1 (PTCH1) and Patched-2 (PTCH2)[7], respectively, both of which are transmembrane receptors that negatively regulate the Hedgehog (Hh) signaling pathway[12]. Despite this homology, several studies have reported that PTCHD1 does not appear to be similarly involved in repressing Hh-dependent signaling[9,13,14]. Likewise, PTCHD1 also exhibits 21.17% sequence homology with the cholesterol-trafficking transmembrane protein Niemann-Pick disease type C1 (NPC1)[7], and has correspondingly been observed to directly bind cholesterol[14]. Finally, numerous protein-protein interactions (PPIs) involving the C-terminal PDZ-binding domain of PTCHD1 have been reported, including proteins within both the postsynaptic density (PSD) and the retromer complex[9,13], potentially indicating a synaptic function of PTCHD1.

Studies have sought to generate inferences regarding the function of PTCHD1 by characterizing the network of neural proteins interacting with its C-terminal PDZ-binding domain. In this study, we have identified and validated a novel PPI between the first lumenal loop of PTCHD1 and the SNARE-associated protein SNAPIN. The clinically-relevant missense mutations within this exoplasmic region of PTCHD1 that were evaluated in this study do not appear to disrupt its ability to interact with SNAPIN. The pathoetiology of these exoplasmic missense variants is apparently unrelated to their interaction with SNAPIN. The mechanism of pathogenicity for several of these missense variants appears to be the result of misfolding-mediated ER retention and impaired membrane localization.

2. Materials and Methods

2.1 Yeast Two-Hybrid Screen

The Matchmaker Gold Yeast Two-Hybrid System (Takara Bio; Kusatsu, Japan) was used. Briefly, lumenal loop 1 (amino acids 49-270) or a fusion of lumenal loop 1 to lumenal loop 2 (amino acids 521-695) of the human ortholog of *PTCHD1* was cloned into the pGBKT7 vector in-frame with the DNA-binding domain of the GAL4 transcription factor. Constructs were separately transformed into the *S. cerevisiae* strain Y2HGold and independently used as bait to probe two separate cDNA libraries fused to the activation domain of GAL4: 1) Mate & Plate Library Mouse Embryo Day 11, and 2) Normalized Mate & Plate Library Adult Human Brain, in three independent screens. Positive clones were selected on synthetic dropout medium in the absence of tryptophan, leucine, histidine, and adenine, and supplemented with X-gal. Positive clones were subjected to plasmid DNA extraction and transformation into *E. coli*, and plasmids from individual colonies were then amplified by PCR and Sanger-sequenced to confirm the correct insert.

2.2 Expression Plasmids

Under the assumption that the functions and interactions of PTCHD1 and SNAPIN are similar across mammalian species, the complete coding sequences of the mouse orthologs of *Ptchd1* and *Snapin*, which exhibit 98.1% and 97.8% sequence homology, respectively, with their human orthologs, were amplified from differentiated P19 mouse embryonal carcinoma cells[15] and ligated into the multiple cloning site of the expression vector pcDNA3.1 myc-His B (Thermo Fisher Scientific; Waltham, MA). *Snapin* was cloned in-frame with the downstream myc-His tags. For *Ptchd1*, the stop codon was included, and a 3xFlag epitope tag was subsequently inserted at the N-terminus by oligonucleotide phosphorylation, annealing, and ligation. Finally, 3xFlag-tagged *Ptchd1* lumenal loop 1 (amino acids 48-266), lumenal loop 2 (amino acid 499-698), and a lumenal loop 1-loop 2 chimeric protein were cloned into pcDNA3.1 myc-His B, succeeded by a stop codon. In the chimeric protein, in order to allow the two lumenal loops to fold independently of one another, they were separated by a short $(Gly_5Ser)_2$ linker. Primer sequences used for expression cloning are provided in **Table S1**.

Site-directed mutagenesis was employed to generate the clinical *Ptchd1* missense variants evaluated in this study. Briefly, the wildtype *3xFlag-Ptchd1-pcDNA3.1* vector was amplified using Q5 high-fidelity DNA polymerase (NEB; Ipswich, MA), with the forward primer containing the mutant codon of interest. Next, purified PCR products were phosphorylated and re-circularized with DNA ligase. All mutant constructs were confirmed by Sanger sequencing (**Figures S1** and **S2**). The human ortholog of *PTCHD1* was recombined into the vector pDEST53 (Thermo Fisher Scientific) in-frame with GFP. For this, Q5 polymerase-amplified *PTCHD1* flanked by attB1 and attB2 sequences was incubated with BP Clonase enzyme mix (Thermo Fisher Scientific) and the donor vector pDONR (Thermo Fisher Scientific). After transformation, plasmid purification, and Sanger sequencing, the resultant donor vector was incubated with LR Clonase enzyme mix (Thermo Fisher Scientific) and the expression vector pDEST53. Primer sequences used for site-directed mutagenesis are provided in **Table S2**.

2.3 Cell Culture

HEK293T cells (ATCC, CRL-3216) were maintained in DMEM supplemented with 10% fetal bovine serum (FBS) (Wisent; Saint-Jean-Baptiste, QC, Canada) and 1% penicillin-streptomycin (Wisent) in T75 flasks (Sarstedt; Nümbrecht, Germany). Cells were passaged every 48-72 hours at semi-confluence by trypsinization (Wisent).

P19 mouse embryonal carcinoma cells (ATCC, CRL-1825) were maintained in α-MEM supplemented with 7.5% newborn calf serum (Gibco; Thermo Fisher Scientific), 2.5% FBS (Wisent), and 1% penicillin-streptomycin (Wisent) in T75 flasks (Sarstedt). Undifferentiated cells were passaged every 48-72 hours at semi-confluence. To induce neuronal differentiation, undifferentiated cells were grown on non-adherent bacterial-grade plates (Thermo Fisher Scientific) supplemented with 1 μM retinoic acid for four days. On the fourth day, aggregates were plated onto sterile coverslips in 12-well plates, and allowed to differentiate for six days.

2.4 Co-immunoprecipitation

HEK293T cells were re-seeded in 6-well culture plates (Falcon; Corning, NY). 24 hours later, Lipofectamine 3000 (Thermo Fisher Scientific) was utilized according to the manufacturer's instructions

to co-transfect 2 µg of *3xFlag-Ptchd1* and 500 ng of *Snapin-myc* expression plasmids. 48 hours later, cells were washed with ice-cold PBS and lysed in immunoprecipitation buffer (50 mM Tris-HCl, pH 8.0, 150 mM NaCl, 1% NP-40) supplemented with cOmplete Mini EDTA-free protease inhibitors (Roche; Basel, Switzerland). Lysates were incubated for 10 minutes on ice, followed by centrifugation at 10,000 x *g* for 10 minutes at 4°C. Supernatants were quantified using the Bradford total protein assay (Bio-Rad; Hercules, CA). For co-immunoprecipitation experiments, 500 µg of lysates were incubated with 1 µg of mouse α-Flag M2 antibody (Sigma-Aldrich #1804; St. Louis, MO) in a final volume of 1 mL of immunoprecipitation buffer overnight at 4°C with rotation. The next day, lysates were incubated with 50 µl of Dynabeads Protein G (Thermo Fisher Scientific) for two hours at room temperature with rotation. Antibody-protein complexes were then separated magnetically, washed three times with PBS, and eluted from the Dynabeads using elution buffer (75 mM Glycine-HCl, pH 2.7). Two biological replicates were performed for co-immunoprecipitation experiments.

2.5 Immunoblotting

Input lysates (5 µg of total protein) and entire elution products were combined with 4x Laemmli buffer (Bio-Rad) supplemented with 10% β-mercaptoethanol. Samples were subsequently incubated at 37°C for 20 minutes to avoid boiling-induced aggregation of multi-pass transmembrane proteins[16]. Samples were separated using 4-15% gradient SDS-PAGE gels (Bio-Rad), transferred to PVDF membranes (Bio-Rad), and blocked in 3% skim milk powder (BioShop; Burlington, ON, Canada) for one hour at room temperature with agitation. Blots were incubated with primary antibodies at the appropriate concentrations in blocking solution overnight at 4°C with agitation. The next day, blots were washed three times with wash buffer (TBS supplemented with 0.2% Tween-20) and incubated with horseradish peroxidase-conjugated secondary antibodies at the appropriate concentrations in blocking solution for one hour at room temperature with agitation. Blots were then washed three additional times with wash buffer, followed by chemiluminescence detection (Thermo Fisher Scientific) using the ChemiDoc imaging system (Bio-Rad). Antibody concentrations are provided in **Table S3**.

2.6 Immunocytochemistry

Sterile 13 mm coverslips (Sarstedt) were inserted into 24-well culture plates (Falcon) and coated with 100 µg/mL poly-D-lysine solution (Sigma-Aldrich #1804) according to the manufacturer's instructions. HEK293T cells were re-seeded at low dilutions onto coated coverslips. The next day, Lipofectamine 3000 (Thermo Fisher Scientific) was utilized according to the manufacturer's instructions to co-transfect 10 ng of *3xFlag-Ptchd1* expression plasmids and 490 ng of the inert carrier plasmid pBV-Luc (addgene.org #16539). 24 hours later, cells were rinsed with PBS and fixed with ice-cold 100% methanol at -20°C for 15 minutes. Cells were then washed twice with PBS and incubated with blocking solution (10% goat serum (Cell Signaling; Danvers, MA) in PBS supplemented with 0.1% Tween-20) for one hour at room temperature with agitation. After blocking, cells were incubated with primary antibodies at the appropriate concentrations in blocking solution overnight in a humidified chamber at 4°C with agitation. The next day, cells were washed three times with PBS and incubated with Alexa Fluor-conjugated secondary antibodies at the appropriate concentrations in blocking solution for one hour at room temperature with agitation in the dark. Cells were then washed three additional times with wash buffer, followed by incubation with NucBlue reagent (Thermo Fisher Scientific) according to the manufacturer's instructions. Finally, cells were mounted on glass slides using Dako mounting medium

(Agilent; Santa Clara, CA). Antibody concentrations are provided in **Table S3**. Three biological replicates were performed for immunocytochemistry experiments.

2.7 Image Acquisition and Analysis

Images were acquired using a Leica TCS SP8 confocal microscope and the Leica Application Suite X (LASX) software. The 405 nm (66.6% intensity), 488 nm (5.2% intensity), and 552 nm (2.0% intensity) lasers were used. Images were acquired sequentially under 63x magnification. For each image, consecutive high-resolution z-stacks were acquired with a z-interval of 0.6 µm. For each Ptchd1 variant, three biological replicates (each consisting of three consecutive z-stacks for 6-7 separate images) were blindly analyzed by an independent technician. Pixel intensity thresholds were adjusted identically for all images: 1) 3xFlag (minimum 30; maximum 255) and 2) Calnexin/At1a (minimum 15; maximum 230). To quantify the overlapping intensity values of 3xFlag-Ptchd1 and Calnexin or At1a, the Pearson correlation coefficient was computed using the JACoP plugin in FIJI using default settings. To calculate statistical significance, a one-way analysis of variance (ANOVA) was used, followed by a Tukey's Honest Significant Difference (HSD) test to compare variants of Ptchd1 with wildtype Ptchd1.

3. Results

3.1 Identification of SNAPIN as a PTCHD1-binding Protein

To identify novel neural proteins that may be putatively interacting with predicted exoplasmic domains of PTCHD1, lumenal loop 1 or a fusion of lumenal loops 1 and 2 were separately used as bait in yeast two-hybrid screens. Subsequent sequencing of positive clones from the screen of lumenal loop 1 against an adult human brain cDNA library indicated that there is a highly successful bait-prey interaction between this region of PTCHD1 and SNAPIN, with 17 hits, compared to the next highest with 2 (**Table S5**). This result was confirmed via co-immunoprecipitation, which revealed that mouse Snapin interacts strongly with the mouse Ptchd1 lumenal loop 1, and very weakly with the lumenal loop 1-loop 2 fusion protein (**Figure 1A**). Finally, to exclude the possibility that the binding between PTCHD1 and SNAPIN is an artificial byproduct of their spontaneous proximity to one another during cell lysis or ectopic expression in yeast cells, immunocytochemistry was used to evaluate their subcellular localization in P19-induced neural cells. Both PTCHD1 and SNAPIN were observed to co-localize within dendritic projections (**Figure 1B**), providing support for a genuine functional interaction.

3.2 Binding of Snapin to Clinical Ptchd1 Lumenal Loop Variants

In order to ascertain if the mechanism of pathogenicity for clinic-identified point mutations within the lumenal loops of PTCHD1 is related to an impaired capacity to bind SNAPIN, co-immunoprecipitation experiments were performed with these variants, using mouse *Ptchd1* and *Snapin* constructs in HEK293T cells. The point mutations within lumenal loops 1 and 2 were identified in the literature[8,10,17,18] as well as in clinical genomics databases[19,20] and through personal communication with clinicians (**Table S4**). It was observed that all variants containing point mutations within lumenal loops 1 and 2 evaluated in this study were both detectable at the protein level and able to interact with Snapin (**Figures 2A** and **2B**). Variations in monomeric protein expression were observed, with the point mutants Pro75Leu, Pro75Gln, Val195Ile, Tyr213Cys, and Phe549Cys exhibiting attenuated protein levels at the expected size relative to wildtype

Ptchd1 (**Figures 2A** and **2B**). Interestingly, expression of all point mutants was apparent in aggregate form at the interphase between the stacking and resolving portions of the SDS-PAGE gels (**Figures 2A** and **2B**).

3.3 Subcellular Localization of Ptchd1 Lumenal Loop Variants

As the pathoetiology of Ptchd1 lumenal loop variants appears to be unrelated to their ability to bind Snapin, efforts next focused on evaluation of their subcellular localization. The point mutants Pro75Leu, Pro75Gln, Val195Ile, Tyr213Cys, Asp527Glu, and Phe549Cys were all observed to demonstrate increased retention within the ER in comparison with wildtype Ptchd1 (**Figure 3**). Mutations at Pro75 appear to be particularly deleterious, with Pro75Leu and Pro75Gln exhibiting 75% and 84% higher associations with the ER marker Calnexin, respectively, than wildtype Ptchd1 (**Figure 3**). Correspondingly, all of these variants with the exception of Asp527Glu were associated with attenuated localization within the cell membrane relative to wildtype Ptchd1 (**Figure 4**). Mutations generating undesirable cysteine residues seemingly impaired cell membrane trafficking to the largest extent, with Tyr213Cys and Phe549Cys displaying 67% and 68% less co-localization with the cell membrane marker At1a, respectively, than wildtype Ptchd1 (**Figure 4**). Similarly, mutations affecting Pro75 considerably impaired the ability of these point mutants to be trafficked to the cell membrane, with co-localization with At1a attenuated in Pro75Leu and Pro75Gln by 43% and 42%, respectively, relative to wildtype Ptchd1 (**Figure 4**).

4. Discussion

Due to the paucity of definitive functional information for PTCHD1, studies have sought to deduce its role by delineating its network of interacting proteins. Affinity purification experiments with adult mouse neural lysates indicate that Ptchd1 binds with the PSD proteins Synapse-associated protein 102 (Sap102), PSD protein 95 (PSD95), Dlg1-3, Magi1, Magi3, and Lin7, as well as with components of the retromer complex Snx27 and Vps26b, and that these interactions are all mediated by the C-terminal PDZ-binding domain[9,13]. To date, the only interaction with Ptchd1 that has been reported to occur independent of the C-terminal PDZ-binding domain is with the retromer complex protein Vps35[13]. Given the predicted multi-pass structure and membrane topology of PTCHD1, it is plausible that in addition to the cytoplasmic C-terminus, the lumenal loops may facilitate further PPIs. In this regard, the present study has identified a novel binding partner, SNAPIN, which demonstrates a high-affinity interaction with the first lumenal loop of PTCHD1.

SNAPIN associates with Synaptosomal-associated protein 25 (SNAP25)[21], which is a core component of the *trans*-SNARE complex, along with Synaptobrevin and Syntaxin[22]. The *trans*-SNARE complex facilitates the exocytosis of neurotransmitter-containing synaptic vesicles following depolarization of pre-synaptic neurons[23]. In *C. elegans*, binding of the SNAPIN ortholog SNPN-1 to SNAP25 stabilizes SNARE complex formation and promotes synaptic vesicle priming[24]. Functionally, primary cortical neurons from Snapin^{null} mice show reduced frequency of miniature excitatory post-synaptic currents, a smaller pool of release-ready synaptic vesicles, and de-synchronized synaptic vesicle fusion[25]. In addition, at the neuromuscular junctions of SNPN-1^{null} *C. elegans*, the amount of docked, fusion-competent vesicles was significantly reduced, although the overall kinetics of synaptic

transmission were unaffected[24]. Finally, the dosage of Snapin in mouse primary hippocampal neurons appears to influence dendritic arborization by its binding to the cytosolic PSD95 interactor Cypin[26] (mouse ortholog of human guanine deaminase, GDA). Collectively, these data indicate that SNAPIN is intimately involved in both neurodevelopment and neurotransmission.

Identification of SNAPIN as a putative PTCHD1 binding partner was obtained from a yeast two-hybrid screen. An inherent limitation with this *in vitro* approach is that it provides artificial opportunities for protein interaction, potentially resulting in false positives as the candidate proteins are expressed ectopically within the same subcellular compartment. Snapin has been found to be expressed ubiquitously in various rat brain subregions, including both the cerebellum and cortex[21], where *PTCHD1/Ptchd1* is highly-abundant at the transcript level[7]. Furthermore, in fractionated rat cerebral synaptosomes, Snapin was exclusively detected in synaptic vesicles[21]. Together, these data are consistent with the subcellular co-localization observed between PTCHD1 and SNAPIN within the dendritic processes of P19-induced neurons in this study (**Figure 1B**). In addition to this neuronal co-localization, the validated binding between Snapin and the first lumenal loop of Ptchd1 (**Figure 1A**) suggests the likelihood of a genuine functional interaction. In Ptchd1, the two lumenal loops are spatially separated by six transmembrane domains and over 230 amino acids, but the two loops in our chimeric protein were only separated by a short $(G_5S)_2$ linker. The weak interaction observed (**Figure 1A**) between Snapin and the loop 1-loop 2 chimeric protein may be due to structural perturbation of the Snapin-binding pocket resulting from abnormal proximity of the two lumenal loops.

Developmentally, Snapin^{null} mutant mice exhibit embryonic lethality[24], whereas Ptchd1 mutant mice are viable, but demonstrate an array of neurodevelopmental abnormalities and ASD-like behaviours[7]. This disparity indicates that in the absence of Ptchd1, Snapin still maintains a sufficient basal level of activity to ensure embryonic survival. Studies have indicated that dysregulation of neurotransmission is implicated in the pathoetiology of ASD[27]. Therefore, PTCHD1 may be involved in coordinating SNAPIN-mediated synaptic vesicle exocytosis, contributing to the precise synchrony of neurotransmission within the brain that is required for proper cognition.

Previous research has reported that point missense variants within the first (Pro32Arg and Pro32Leu) and third (Gly300Arg and Ala310Pro) transmembrane domains were associated with decreased protein expression, ER retention, and impaired plasma membrane trafficking[10]. Mutations of polar or ionizable residues within transmembrane domains are particularly deleterious to proteins[28]. This study focused solely on nonsynonymous variants within the soluble exoplasmic loops of Ptchd1. Ten of the lumenal loop 1 and loop 2 missense variants were detectable in monomeric form at varying levels (**Figures 2A** and **2B**). This is in contrast to Halewa et al., which reported marked instability of the Lys181Thr point mutant[10], which was not observed in this study. This discrepancy may be attributable to differences in the epitope tag, transfection conditions, or the length of the post-transfection incubation period prior to cell lysis. The two missense variants that generated non-canonical cysteine residues, Tyr213Cys and Phe549Cys, were only detectable in aggregate form (**Figures 2A** and **2B**), possibly due to the formation of disulfide bridge cross-linked homodimers. Finally, the two variants involving mutated proline residues, Pro75Leu and Pro75Gln, as well as the variant Val195Ile, appeared to demonstrate reduced monomeric protein expression (**Figure 2A**). Within a protein, the conformational rigidity of proline residues confers unique local secondary structure, with the cyclic nature of proline side chains anchoring the dihedral angle

φ at approximately -65 degrees[29]. Consequently, substitutions generating or abolishing proline residues may result in relatively pronounced local conformational changes in comparison with other types of substitutions[30], leading to protein misfolding and aggregation.

Amino acid residues corresponding to the missense variants assayed in this study appear to be evolutionarily conserved, with only Ser51 and Gln102 deviating from the corresponding ortholog in zebrafish (**Figure S3**). Interestingly, both the Ser51Asn and Gln102Arg missense mutations analyzed in this study corresponded to the initial amino acid residues at these positions in zebrafish, indicating some degree of structural flexibility between these pairs of residues. Despite this apparent conservation, the interaction between Snapin and the first lumenal loop of Ptchd1 was not abolished by any of the nine clinical point mutations evaluated in this study (**Figure 2A**). This implies that the SNAPIN-binding domain of PTCHD1 is not structurally reliant on these specific amino acid residues. Furthermore, these missense variants do not appear to alter the secondary or tertiary structure of the first lumenal loop to impede binding with Snapin.

Clinically, these data suggest that the pathoetiologies of the missense variants evaluated in this study are unrelated to their interaction with SNAPIN. PTCHD1 localizes within the plasma membrane in non-neuronal cells[8,10,13], and in neurons is trafficked to the postsynaptic density[9,13]. PDZ domains have been implicated in the organization of protein complexes at the plasma membrane[31], and the localization of PTCHD1 in dendritic spines is correspondingly dependent upon its short C-terminal PDZ-binding domain (Ile-Thr-Thr-Val)[9]. Immunocytochemical analyses revealed that several of the missense variants analyzed in this study (Pro75Leu, Pro75Gln, Val195Ile, Tyr213Cys, Asp527Glu, and Phe549Cys) displayed apparent retention by the ER (**Figure 3**). Consistent with this, five of these ER-retained missense variants also exhibited decreased plasma membrane localization, with the only exception being Asp527Glu (**Figure 4**). Collectively, these data offer a pathoetiological mechanism for these missense variants, in which protein misfolding-mediated aggregation and retention in the rough ER and subsequent impaired plasma membrane trafficking leads to insufficient bioavailable PTCHD1. The mechanism of pathogenicity for the other missense variants evaluated in this study that displayed canonical subcellular localization (Ser51Asn, Leu73Phe, Gln102Arg, Val150Met, Lys181Thr, and Thr602Ala) remains elusive. Loop regions of transmembrane proteins constitute binding pockets for interacting proteins and other biomarkers[32]. Therefore, it is feasible that the binding of either cholesterol or an as yet unidentified PTCHD1 interacting partner may be affected by these point mutations.

The model system for analyses of exogenous protein subcellular localization in this study is HEK293T cells due to their high transfection efficiency, robust translation of exogenous proteins, and reproducibility of results. A constraint with this system, however, is that it is non-neuronal, which may affect the translatability of findings to a neuronal context. This concern is alleviated by the fact that mechanisms of retention of misfolded proteins by the rough ER are highly conserved across cell types. In addition, this system has previously been used to evaluate the subcellular localization of PTCHD1 missense variants[10].

Despite the fact that *PTCHD1* is an established susceptibility gene for ASD and ID, very little is known regarding its function in the brain. In addition, the pathoetiology of several rare patient-associated missense variants is currently unknown. This study has identified and validated a novel PTCHD1 interacting partner, SNAPIN, which binds to the first lumenal loop. We have also confirmed that clinical

missense variants within the first and second exoplasmic loops of PTCHD1 do not abolish binding with SNAPIN. Finally, we report several clinically-relevant missense variants that exhibit ER retention and impaired plasma membrane localization. Collectively, these data deliver insights regarding the possible role of PTCHD1 in neurodevelopment, as well as offer mechanisms regarding the pathoetiology of clinical missense variants, providing a platform for future diagnostic assays, and for improved interpretation of PTCHD1 variants of uncertain significance by genetic diagnosticians. It may also inform screening for corrective pharmacological interventions. Future research should be aimed at clarifying the effects of PTCHD1 on SNAPIN-mediated synaptic vesicle exocytosis, as well as further elucidating the endogenous network of proteins interacting with PTCHD1.

Acknowledgements – This work was supported by a grant from the Canadian Institutes of Health Research to J.B.V. (#PJT-156367).

Author Contributions – S.F.P., C.T.Y.X., P.A.H., and J.B.V. conceptualized the study; S.F.P., C.T.Y.X., and S.C.E. performed the experiments; T.M. blindly analyzed the co-localization data; S.F.P. and J.B.V. analyzed the data and wrote the manuscript.

Conflict of Interest – CAMH and J.B.V. hold intellectual property rights and a license for diagnostic testing for *PTCHD1* with Quest Diagnostics. All other authors report no conflict of interest.

References

1. Hirota, T. & King, B. H. Autism Spectrum Disorder: A Review. *JAMA* **329**, 157–168 (2023).
2. Zeidan, J. *et al.* Global prevalence of autism: A systematic review update. *Autism Res* **15**, 778–790 (2022).
3. Loomes, R., Hull, L. & Mandy, W. P. L. What Is the Male-to-Female Ratio in Autism Spectrum Disorder? A Systematic Review and Meta-Analysis. *J Am Acad Child Adolesc Psychiatry* **56**, 466–474 (2017).
4. Simonoff, E. *et al.* Psychiatric disorders in children with autism spectrum disorders: prevalence, comorbidity, and associated factors in a population-derived sample. *J Am Acad Child Adolesc Psychiatry* **47**, 921–929 (2008).
5. Tick, B., Bolton, P., Happé, F., Rutter, M. & Rijsdijk, F. Heritability of autism spectrum disorders: a meta-analysis of twin studies. *J Child Psychol Psychiatry* **57**, 585–595 (2016).
6. Marshall, C. R. *et al.* Structural variation of chromosomes in autism spectrum disorder. *Am J Hum Genet* **82**, 477–488 (2008).

7. Pastore, S. F., Ko, S. Y., Frankland, P. W., Hamel, P. A. & Vincent, J. B. PTCHD1: Identification and Neurodevelopmental Contributions of an Autism Spectrum Disorder and Intellectual Disability Susceptibility Gene. *Genes (Basel)* **13**, 527 (2022).
8. Noor, A. *et al.* Disruption at the PTCHD1 Locus on Xp22.11 in Autism spectrum disorder and intellectual disability. *Sci Transl Med* **2**, 49ra68 (2010).
9. Ung, D. C. *et al.* Ptchd1 deficiency induces excitatory synaptic and cognitive dysfunctions in mouse. *Mol Psychiatry* **23**, 1356–1367 (2018).
10. Halewa, J. *et al.* Novel missense mutations in PTCHD1 alter its plasma membrane subcellular localization and cause intellectual disability and autism spectrum disorder. *Hum Mutat* **42**, 848–861 (2021).
11. Xie, C. T. Y., Pastore, S. F., Vincent, J. B., Frankland, P. W. & Hamel, P. A. *Nonsynonymous Mutations in Intellectual Disability and Autism Spectrum Disorder Gene PTCHD1 Disrupt N-Glycosylation and Reduce Protein Stability*. http://biorxiv.org/lookup/doi/10.1101/2022.09.23.509248 (2022) doi:10.1101/2022.09.23.509248.
12. Hu, A. & Song, B.-L. The interplay of Patched, Smoothened and cholesterol in Hedgehog signaling. *Curr Opin Cell Biol* **61**, 31–38 (2019).
13. Tora, D. *et al.* Cellular Functions of the Autism Risk Factor PTCHD1 in Mice. *J Neurosci* **37**, 11993–12005 (2017).
14. Hiltunen, M. K. *et al.* PTCHD1 Binds Cholesterol but Not Sonic Hedgehog, Suggesting a Distinct Cellular Function. *Int J Mol Sci* **24**, 2682 (2023).
15. McBurney, M. W. & Rogers, B. J. Isolation of male embryonal carcinoma cells and their chromosome replication patterns. *Dev Biol* **89**, 503–508 (1982).

16. Fleet, A. J. & Hamel, P. A. The protein-specific activities of the transmembrane modules of Ptch1 and Ptch2 are determined by their adjacent protein domains. *J Biol Chem* **293**, 16583–16595 (2018).
17. Torrico, B. *et al.* Contribution of common and rare variants of the PTCHD1 gene to autism spectrum disorders and intellectual disability. *Eur J Hum Genet* **23**, 1694–1701 (2015).
18. Karaca, E. *et al.* Genes that Affect Brain Structure and Function Identified by Rare Variant Analyses of Mendelian Neurologic Disease. *Neuron* **88**, 499–513 (2015).
19. Landrum, M. J. *et al.* ClinVar: improving access to variant interpretations and supporting evidence. *Nucleic Acids Res* **46**, D1062–D1067 (2018).
20. Firth, H. V. *et al.* DECIPHER: Database of Chromosomal Imbalance and Phenotype in Humans Using Ensembl Resources. *Am J Hum Genet* **84**, 524–533 (2009).
21. Ilardi, J. M., Mochida, S. & Sheng, Z. H. Snapin: a SNARE-associated protein implicated in synaptic transmission. *Nat Neurosci* **2**, 119–124 (1999).
22. Pevsner, J. *et al.* Specificity and regulation of a synaptic vesicle docking complex. *Neuron* **13**, 353–361 (1994).
23. Hu, C. *et al.* Fusion of cells by flipped SNAREs. *Science* **300**, 1745–1749 (2003).
24. Yu, S.-C., Klosterman, S. M., Martin, A. A., Gracheva, E. O. & Richmond, J. E. Differential roles for snapin and synaptotagmin in the synaptic vesicle cycle. *PLoS One* **8**, e57842 (2013).
25. Pan, P.-Y., Tian, J.-H. & Sheng, Z.-H. Snapin facilitates the synchronization of synaptic vesicle fusion. *Neuron* **61**, 412–424 (2009).
26. Chen, M. *et al.* A novel role for snapin in dendrite patterning: interaction with cypin. *Mol Biol Cell* **16**, 5103–5114 (2005).
27. Marotta, R. *et al.* The Neurochemistry of Autism. *Brain Sci* **10**, 163 (2020).

28. Partridge, A. W., Therien, A. G. & Deber, C. M. Missense mutations in transmembrane domains of proteins: phenotypic propensity of polar residues for human disease. *Proteins* **54**, 648–656 (2004).
29. Morris, A. L., MacArthur, M. W., Hutchinson, E. G. & Thornton, J. M. Stereochemical quality of protein structure coordinates. *Proteins* **12**, 345–364 (1992).
30. Li, M., Petukh, M., Alexov, E. & Panchenko, A. R. Predicting the Impact of Missense Mutations on Protein-Protein Binding Affinity. *J Chem Theory Comput* **10**, 1770–1780 (2014).
31. Fanning, A. S. & Anderson, J. M. PDZ domains: fundamental building blocks in the organization of protein complexes at the plasma membrane. *J Clin Invest* **103**, 767–772 (1999).
32. Feller, S. M. & Lewitzky, M. What's in a loop? *Cell Commun Signal* **10**, 31 (2012).

Figure Legends

Figure 1. Interaction and neuronal co-localization between PTCHD1 and SNAPIN.
A) Immunoblot image following co-immunoprecipitation of 3xFlag-tagged Ptchd1 loop 1, loop 2, or a loop1-loop 2 chimera (*top blot*) and myc-tagged Snapin (*bottom blot*). **B)** Immunocytochemical staining of transiently-expressed GFP-tagged PTCHD1 and myc-tagged SNAPIN in P19-induced neurons (day 6 post-induction). Arrows indicate a region along the dendritic process where PTCHD1 and SNAPIN exhibit co-localization.

Figure 2. Binding of clinical PTCHD1 missense variants and SNAPIN.
Immunoblot images following co-immunoprecipitation of 3xFlag-tagged Ptchd1 missense variants (*top blots*) and myc-tagged Snapin (*bottom blots*) in **A)** lumenal loop 1 and **B)** lumenal loop 2. Input blots are displayed above their respective co-immunoprecipitation blot.

Figure 3. ER retention of PTCHD1 missense variants.
A) Pearson correlation coefficient of overlapping pixel intensities between transiently-expressed 3xFlag-tagged Ptchd1 and endogenous Calnexin (ER marker). Data are expressed as the mean ± SEM, and each missense variant was normalized to wildtype Ptchd1. Data were analyzed using a one-way ANOVA followed by a Tukey's HSD test (*$p < 0.05$; **$p < 0.01$; *** $p < 0.001$; **** $p < 0.0001$; n = immunocytochemical co-staining experiments from three separate transfections with 6-7 images captured per staining). **B)** Representative fluorescent images taken for each missense variant.

Figure 4. Impaired plasma membrane trafficking of PTCHD1 missense variants.
A) Pearson correlation coefficient of overlapping pixel intensities between transiently-expressed 3xFlag-tagged Ptchd1 and endogenous At1a (plasma membrane marker). Data are expressed as the mean ± SEM, and each missense variant was normalized to wildtype Ptchd1. Data were analyzed using a one-way ANOVA followed by a Tukey's HSD test (*$p < 0.05$; **$p < 0.01$; *** $p < 0.001$; **** $p < 0.0001$; n = immunocytochemical co-staining experiments from three separate transfections with 6-7 images captured per staining). **B)** Representative fluorescent images taken for each missense variant.

Figure S1. Site-directed mutagenesis of Ptchd1 lumenal loop 1 missense variants.

Figure S2. Site-directed mutagenesis of Ptchd1 lumenal loop 1 missense variants.

Figure S3. Evolutionary sequence alignments of Ptchd1 lumenal loops 1 and 2.
Evolutionary sequence alignments of Ptchd1 **A)** lumenal loop 1 and **B)** lumenal loop 2. Residues corresponding to missense variants are indicated in black.

Table S1. Primers used to generate the expression constructs, along with the corresponding annealing temperatures. Restriction enzyme recognition sequences are underlined. Start and stop codons are shown in green and red, respectively.

Primer	Sequence	Annealing Temperature
BamHI_Ptchd1_F	5'-TACCGGATCCATGCTGCGGCAGGTTCTGC-3'	70°C
AgeI_Ptchd1_R	5'-TACCACCGGTTCACACTGTGGTTATTTGGTCAACCAC-3'	
BamHI_Loop 1_F	5'-TACCGGATCCATGGTCGAAGAGAGCGTGGAGCAC-3'	72°C
AgeI_Loop 1_R	5'-TACCACCGGTTCAACGGCTGGTCTTCTGGAAATCTTCC-3'	
BamHI_Loop 2_F	5'-TACCGGATCCATGTATGTCAAGCCTTTTGTAGTCCTCTTTTACC-3'	69°C
AgeI_Loop 2_R	5'-TACCACCGGTTCAGGCTCCCAGAGAGGAGGC-3'	
NheI_Loop 1_R	5'-TACCGCTAGCACGGCTGGTCTTCTGGAAATCTTCC-3'	72°C
NheI_Loop 2_F	5'-TACCGCTAGCTATGTCAAGCCTTTTGTAGTCCTCTTTTACC-3'	69°C
attB1_PTCHD1_F	5'-ACAAGTTTGTACAAAAAAGCAGGCTATGCTGCGGCAGGTTCTGC-3'	72°C
attB2_PTCHD1_R	5'-ACCCAGCTTTCTTGTACAAAGTGGTTCACACTGTTGTAATTTGGTCA ACCACACGG-3'	
HindIII_3xFlag_Link_F	5'-AGCTTATGGACTACAAGGACCACGACGGTGACTACAAGGACCACGACATCGACTACAAGGA CGACGACGACAAGGGAGGTGGCGGAGGTTCCGGG-3'	
BamHI_3xFlag_Link_R	5'-GATCCCCGGAACCTCCGCCACCTCCCTTGTCGTCGTCGTCCTTGTAGTCGATGTCGTGGTCCT TGTAGTCACCGTCGTGGTCCTTGTAGTCCATA -3'	

Table S2. Primers used for site-directed mutagenesis, along with the corresponding annealing temperature. Mutant codons are shown in red.

Location	Mutation	Sequence	Anneal Temperature
Loop 1	S51N	F: AATGTGGAGCACCTGCTGGCG R: CTCTTCGACCTGGTAGCGGC	72°C
	L73F	F: TTCTTCCCGGTCAACCGCTCCAAG R: GCTGTTGACTAGGTTGCGCTCGATC	72°C
	P75L	F: CTTGTCAACCGCTCCAAGCACCG R: GAAGAGGCTGTTGACTAGGTTGCG	71°C
	P75Q	F: CAAGTCAACCGCTCCAAGCACCG R: GAAGAGGCTGTTGACTAGGTTGCG	71°C
	Q102R	F: CGTAAAGCCAACATGCTAGACCAAC R: GTAGGAGGTGACAATGACCCG	67°C
	V150M	F: ATGGATGACATAGTACACGTCC R: AATGCAAGTCTTATCATTATTCAGGAC	60°C
	V195I	F: ATTACTGTGCACAGCAAGGATCGG R: ACCTCCGAGTTGGTGCCCATTATAC	71°C
	K181T	F: ACGGATGGAAGGGCTGTGTATAATG R: TAAGTGAGTGATCGGATATGTG	62°C
	Y213C	F: TGTTATCTGCAATCAATCAACAGTCTC R: GGTAAGCTGAATGGCCTCTG	63°C
Loop 2	D527E	F: GAACTTAGTAACATCGTAGCAACTGCA R: TGACCCTTCACTGACCTG	65°C
	F549C	F: TGCAACAACTACAGTCCTGTTATTGGG R: GTACTTTTGGTGGGCAGTAG	64°C
	T602A	F: GCAGACTTGCCTAAGAAAAATTTCACAGACATG R: GGACACATTGAGTTTCCGAAGATAATTTAAATAGC	67°C

Table S3. Antibodies used for western blotting and immunocytochemistry, along with the product information and dilution factors.

Experiment	Antibody (Conjugate)	Source	Dilution
Immunoprecipitation; Immunoblotting	Mouse α-Flag	Sigma-Aldrich #1804	1:250 (IP)
	Rabbit α-DYKDDDDK	Cell Signaling #14793	1:750
	Rabbit α-myc	Cell Signaling #2278	1:750
	Goat α-mouse (HRP)	Promega #W402B	1:2500
	Goat α-rabbit (HRP)	Promega #W401B	1:2500
Immunocytochemistry	Mouse α-Flag	Sigma-Aldrich #1804	1:300
	Rabbit α-At1a	Abcam #76020	1:500
	Rabbit α-Calnexin	Abcam #92573	1:1000
	Goat α-rabbit (Alexa Fluor 594)	Thermo Fisher #A11001	1:1000
	Goat α-mouse (Alexa Fluor 488)	Thermo Fisher #A11012	1:1000

Table S4. Location, clinical information, and reference for the missense variants.

Mutation	Location	Clinical Features	Source
S51N	Loop 1	ID	Torrico et al. (2015)
L73F		ASD	Noor et al. (2010)
P75L		ASD	MSSNG (ID # AU3951302)
P75Q		ASD	MSSNG (ID # AU3794302)
Q102R		ID	Personal communication
V150M		Susceptibility to ASD	ClinVar (VCV001334078.1)
K181T		Seizures	Karaca et al. (2015)
V195I		ASD, severe language delay	Noor et al. (2010)
Y213C		Developmental delay	Halewa et al. (2021)
D527E	Loop 2	ASD	Firth et al. (2009)
F549C		ASD	Personal communication
T602A		Unknown	ClinVar (VCV001303783.2)

Table S5. Full **r**esults from the yeast two-hybrid screen.

Protein	Screen	Frequency of Hits
COX11	PTCHD1^{L1-L2} vs. E11 Mouse Embryo cDNA Library	3
MATH1		2
PAX3		1
A2M	PTCHD1^{L1} vs. Adult Human Brain cDNA Library	2
ANKD49		1
ANKRD55		2
ATG5		1
CPLX2		1
DCAF17		1
EPB41L1		1
GFM2		1
HSPD1		1
KDM1A		1
KLHL32		1
METAP2		1
NOL4		1
PDZD2		1
PON		1
PSMD14		1
SNAPIN		17
STMN2		1
SYNE1		1
TADA1		1
TTC8		1
YWHAZ		1
ZnF277		2
ZnF350		1

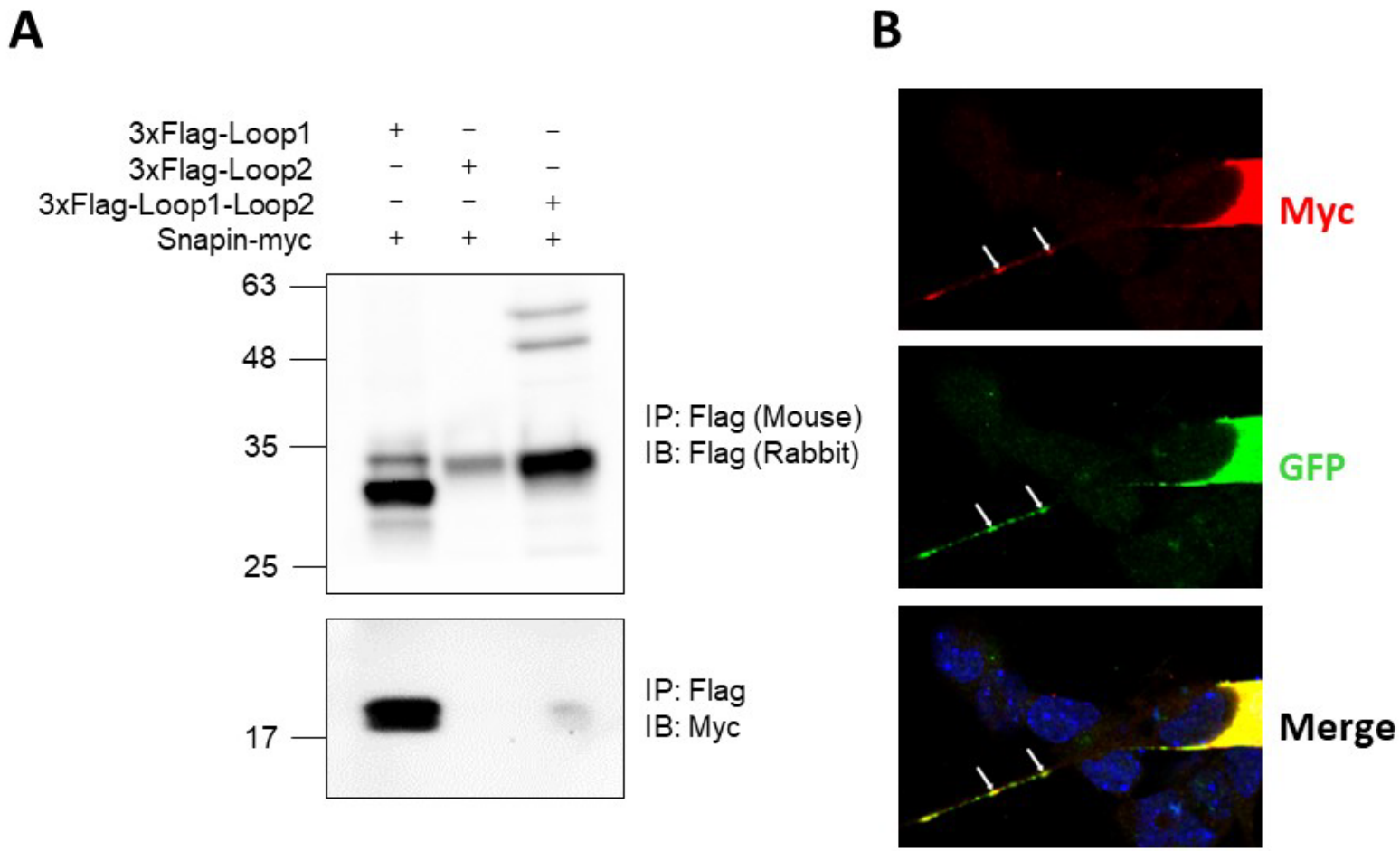
A
3xFlag-Loop1 + − −
3xFlag-Loop2 − + −
3xFlag-Loop1-Loop2 − − +
Snapin-myc + + +
63
48
35
25
IP: Flag (Mouse)
IB: Flag (Rabbit)
17
IP: Flag
IB: Myc
B
Myc
GFP
Merge

Figure 1

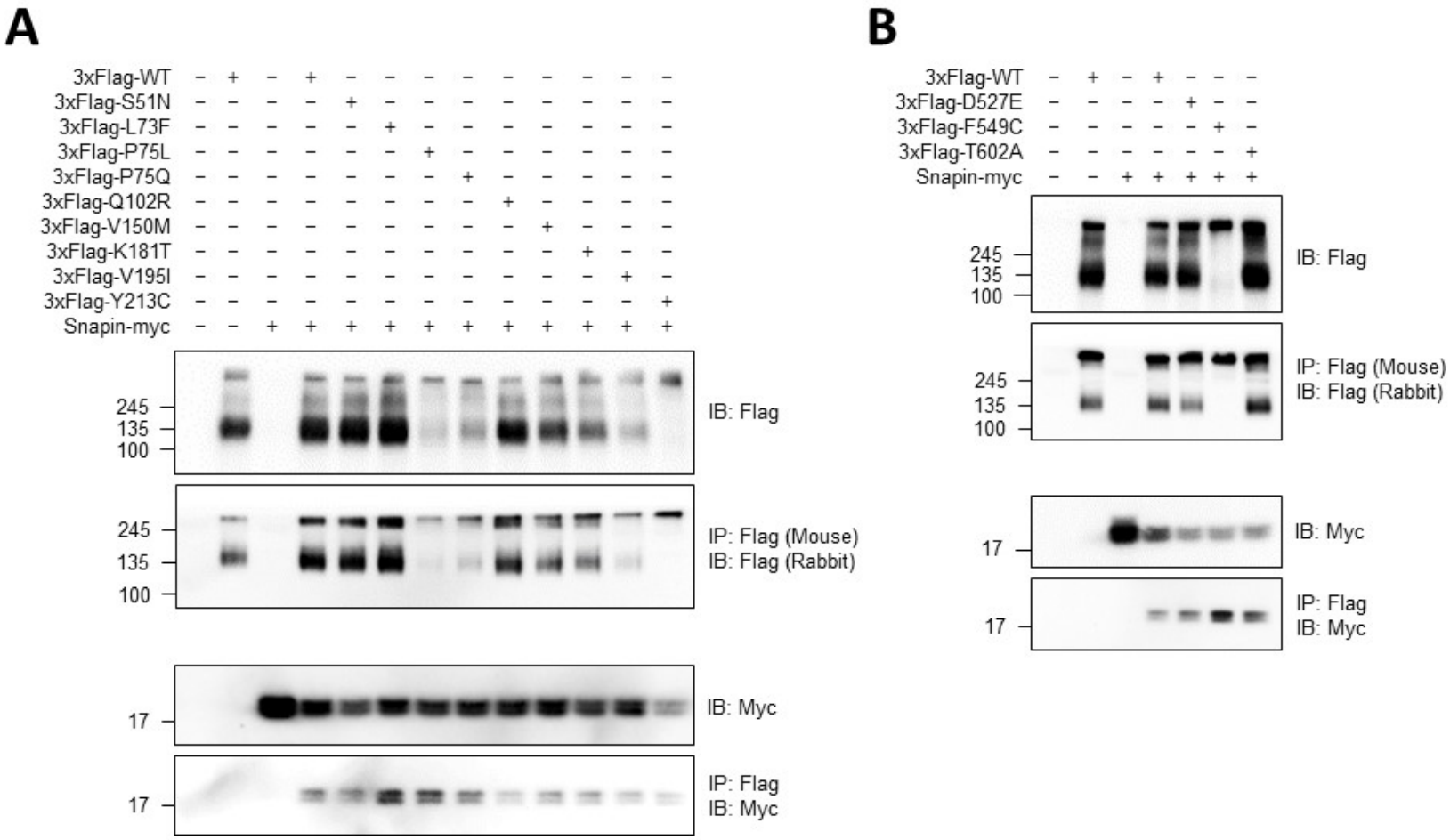
A
3xFlag-WT
3xFlag-S51N
3xFlag-L73F
3xFlag-P75L
3xFlag-P75Q
3xFlag-Q102R
3xFlag-V150M
3xFlag-K181T
3xFlag-V195I
3xFlag-Y213C
Snapin-myc
245
135
100
IB: Flag
IP: Flag (Mouse)
IB: Flag (Rabbit)
17
IB: Myc
IP: Flag
IB: Myc
B
3xFlag-WT
3xFlag-D527E
3xFlag-F549C
3xFlag-T602A
Snapin-myc
245
135
100
IB: Flag
IP: Flag (Mouse)
IB: Flag (Rabbit)
17
IB: Myc
IP: Flag
IB: Myc

Figure 2

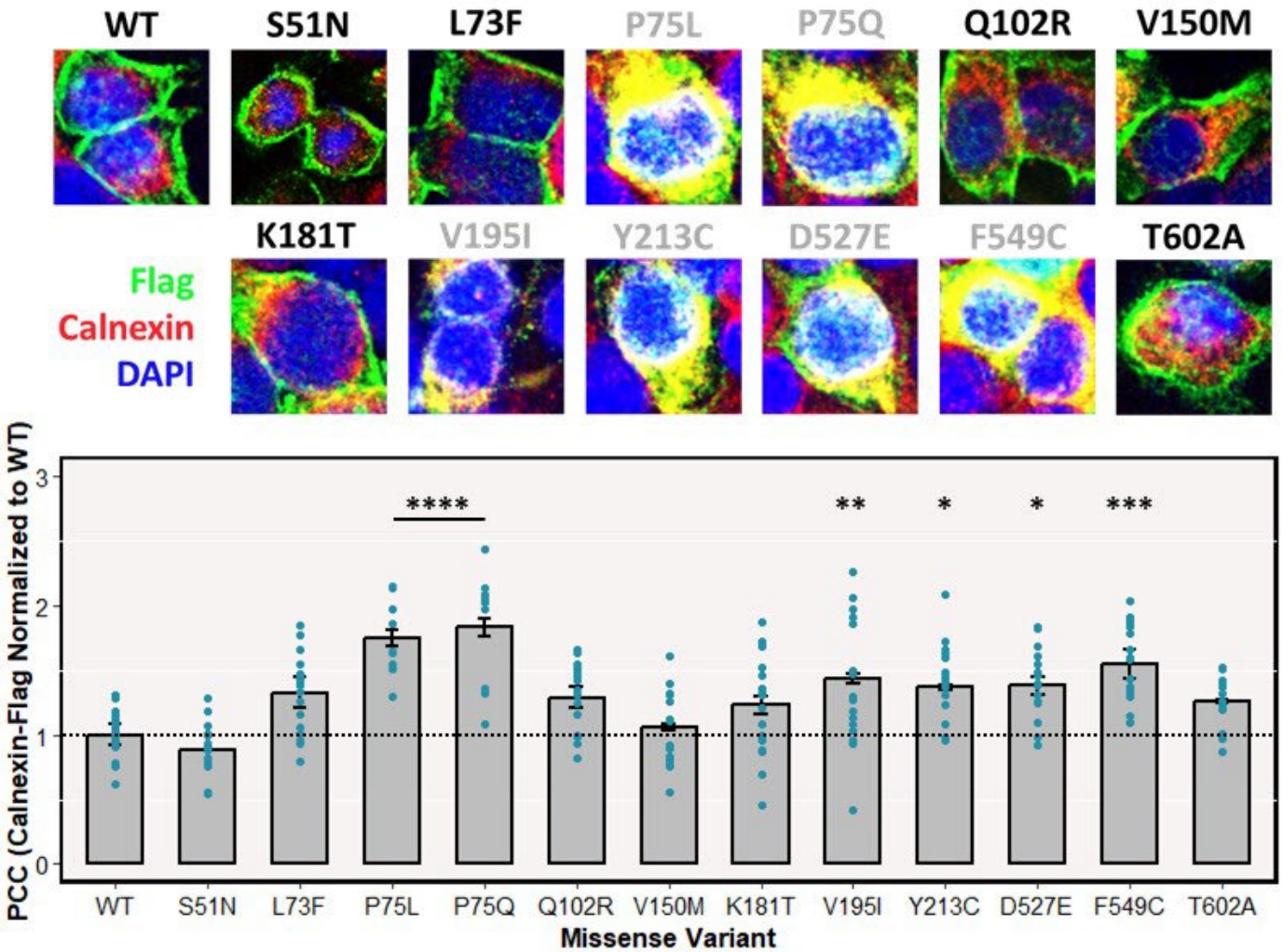
WT
S51N
L73F
P75L
P75Q
Q102R
V150M
K181T
V195I
Y213C
D527E
F549C
T602A
Flag
Calnexin
DAPI
PCC (Calnexin-Flag Normalized to WT)
Missense Variant
****
**
*
*
***

Figure 3

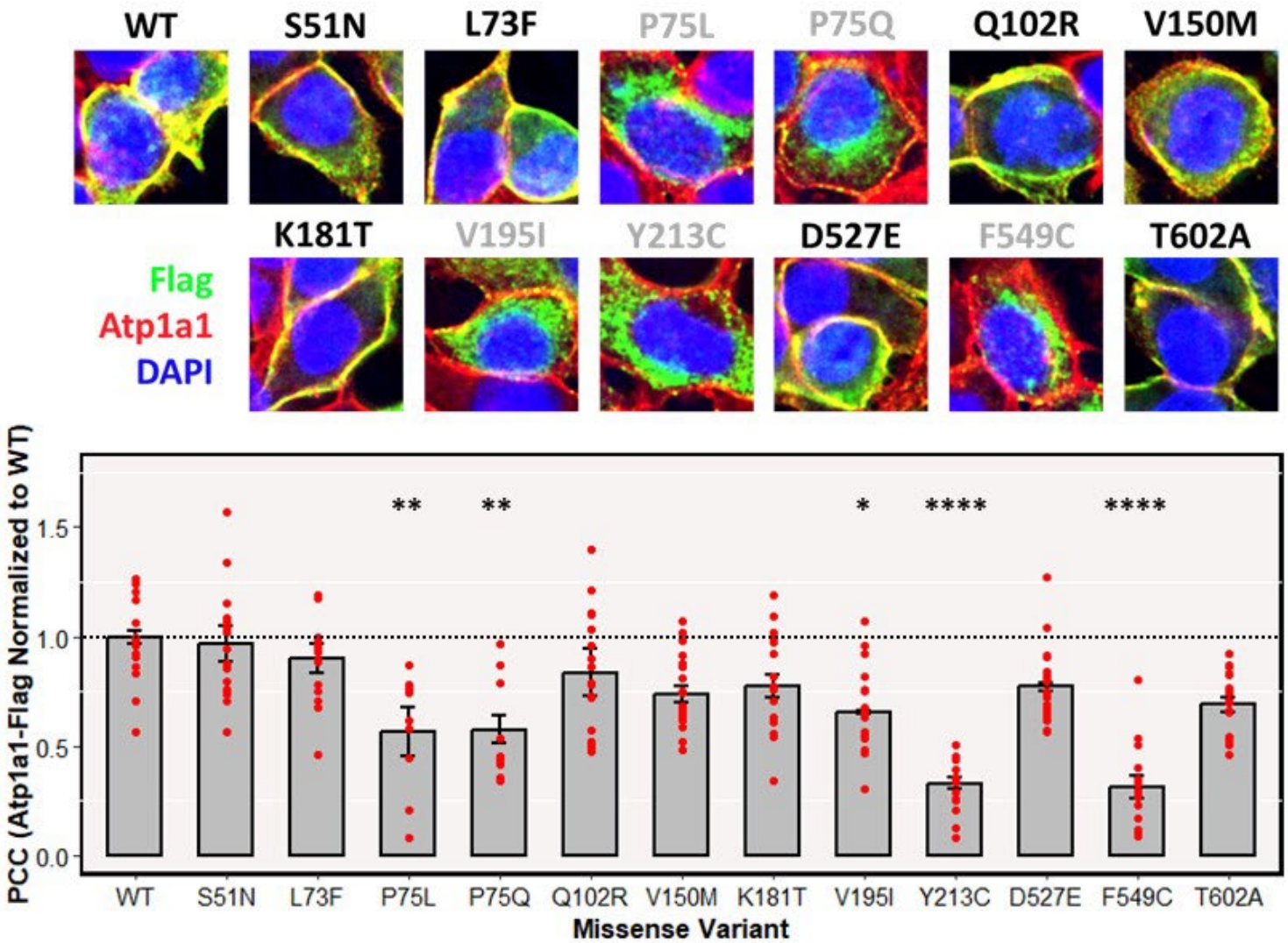
WT
S51N
L73F
P75L
P75Q
Q102R
V150M
K181T
V195I
Y213C
D527E
F549C
T602A
Flag
Atp1a1
DAPI
PCC (Atp1a1-Flag Normalized to WT)
1.5
1.0
0.5
0.0
**
**
*
****
****
WT
S51N
L73F
P75L
P75Q
Q102R
V150M
K181T
V195I
Y213C
D527E
F549C
T602A
Missense Variant

Figure 4